ACCURATE LOCATION OF FAULTS ON THREE-TERMINAL LINE WITH USE OF THREE-END UNSYNCHRONISED MEASUREMENTS

Jan Izykowski
Eugeniusz Rosolowski, Rafal Molag
Wroclaw University of Technology, Wroclaw, Poland
jan.izykowski@pwr.wroc.pl
eugeniusz.rosolowski@pwr.wroc.pl
rafal.molag@wp.pl

Przemyslaw Balcerek
Marek Fulczyk
ABB Corporate Research Center
Krakow, Poland
przemyslaw.balcerek@pl.abb.com
marek.fulczyk@pl.abb.com

Murari Mohan Saha
ABB AB
Västerås, Sweden
murari.saha@se.abb.com

Abstract – This paper presents a new fault location algorithm for three-terminal line utilising unsynchronised measurements of three-end currents and voltages. The distributed parameter line model is strictly considered for formulating three subroutines of the algorithm. Efficient procedure for selecting the valid results is introduced. The presented results of the ATP-EMTP evaluation prove the validity of the fault location algorithm and its high accuracy.

Keywords: three-terminal power line, fault location, three-end unsynchronised measurements, ATP-EMTP

1 INTRODUCTION

Accurate location of faults on overhead power lines for the inspection-repair purpose [1]–[9] is of vital importance for operators and utility staff for expediting service restoration, and thus to reduce outage time, operating costs and customer complains.

Different fault location algorithms for three-terminal lines (Fig. 1), have been developed so far [1]–[8]. The cited algorithms are based on an impedance principle, making use of the fundamental frequency voltages and currents. They differ each other mainly with respect to the applied input signals of the fault locator.

In [1] usage of synchronised measurements of currents and voltages from all three terminals has been considered. Distributed parameter models of the line sections have been utilised there. This assures high accuracy of fault location, and the faulted line section is also reliably indicated [1].

Use of three-end unsynchronised measurements of currents and voltages has been considered in [2]. The lumped models of the line sections were applied there and it was also implied that the error resulting from such simplification is minimised due to the redundancy of the fault location equations. Yet another utilisation of three-end unsynchronised measurements has been proposed in [3], where exchanging the minimal amount of information between the line terminals over a protection channel was considered.

In turn, a demand and importance of developing fault location algorithms for three-terminal lines utilising only two-end synchronised measurements of voltages and currents has been stated in [4].

Limited availability of measurements for fault location on three-terminal lines was considered in [5]–[7]. In [5]–[6] ensure complete immunity to saturation of current transformers (CTs), since only voltage signals are utilised for fault location. The method presented in [7] is based on using minimal amount of measured signals.

In [8] use of three-phase current from all three line terminals and additionally three-phase voltage, acquired at the terminal at which the fault locator is installed, has proposed. Such specific availability of measurements has been assumed with the aim of simple supplementing of the fault location function to current differential relays protecting a three-terminal line.

In this paper, an algorithm, which utilises unsynchronised measurements of currents and voltages at all three terminals is presented. It is assumed, that analytical synchronisation of such measurements has to be performed without resorting to synchronising with the pre-fault measurements. In order to assure high accuracy of fault location, the distributed parameter line model is strictly utilised .

The paper starts with derivation of the fault location algorithm. Then, the sample results of extensive ATP-EMTP [10] evaluation of the algorithm are presented and discussed.

2 FAULT LOCATION ALGORITHM

2.1 Basics of fault location algorithm

The circuit diagram of a three-terminal line for considering the fault location using three-end unsynchronised measurements is presented in Fig. 1. Different types of symmetrical components of the signals can be processed in the algorithm. In Fig. 1, and also further, the signal type is marked by the subscript *i*.

In Fig. 1 the measurements from the end B are taken as the basis, while the measurements from the buses A and C have to be analytically synchronised, with use of the synchronisation operators $e^{j\delta_{Ai}}$ and $e^{j\delta_{Ci}}$, respectively. Thus, two additional unknowns: synchronisation angles δ_{Ai} and δ_{Ci} appear, in comparison to the case of synchronised measurements [1].

The fault can occur at any of three line sections (faults: FA, FB or FC in Fig. 1). The distance to the

particular fault, counted from the particular bus (A, B or C) up to the fault point is marked as: d_{Ai}, d_{Bi}, d_{Ci}, respectively. So, there are three hypotheses regarding placement of the fault in particular line section: AT, BT or CT. All three hypotheses regarding indication of the faulted line section are considered and after calculating the distances to fault (d_{Ai}, d_{Bi}, d_{Ci}) by using these three subroutines, the judgement on selecting only one solution (the valid solution), which is consistent with the actual fault, is performed.

All three subroutines of the presented fault location algorithm are based on the two-end unsynchronised fault location algorithm presented in [9].

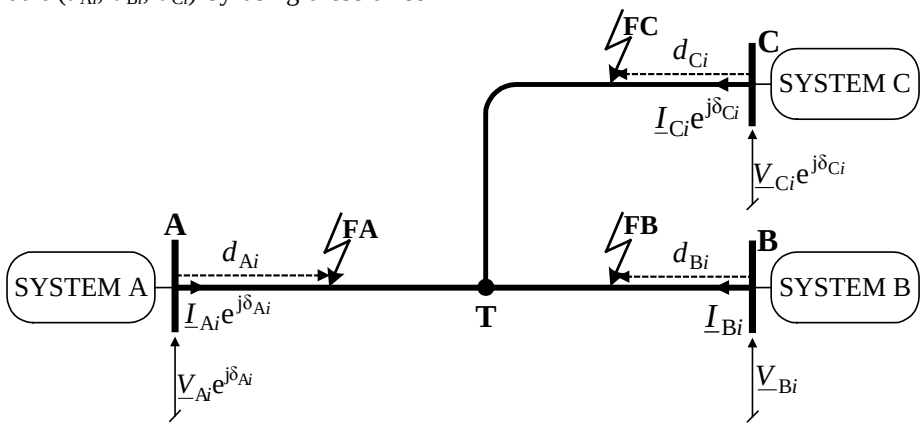

Figure 1: Fault location on three-terminal line using three-end unsynchronised measurements of the *i*–th symmetrical component of voltages and currents.

2.2 Fault location algorithm for two-terminal line

The algorithm from [9] is formulated for the *i*-th symmetrical components and considers both the lumped (Fig. 2) and the distributed parameter (Fig. 3) models of a two-terminal power line.

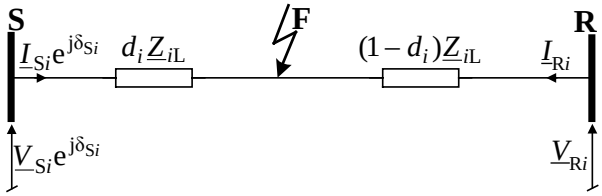

Figure 2: Lumped model of faulted line for considering unsynchronised two-end fault location.

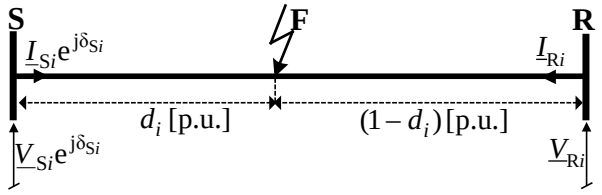

Figure 3: Distributed parameter model of faulted line for considering unsynchronised two-end fault location.

The input signals of the two-end unsynchronised fault location algorithm are: $\underline{V}_{Si}$, $\underline{V}_{Ri}$, $\underline{I}_{Si}$, $\underline{I}_{Ri}$ – voltage and current phasors from the terminals S and R, respectively, for the *i*-th symmetrical component. Digital measurements of the phasors from two line ends are considered as the unsynchronised. Therefore, the measurements from the terminal R are assumed as the basis, while the phasors from the end S are analytically synchronised – with use of the synchronisation operator:

$$e^{j\delta_{Si}} = \cos(\delta_{Si}) + j\sin(\delta_{Si}) \tag{1}$$

The unknowns of the fault location algorithm are:

d_i – distance to fault from bus S (p.u.),

δ_{Si} – synchronisation operator.

If the lumped line model (Fig. 2) is considered, the parameter: $\underline{Z}_{iL}$ – impedance of the line SR, for the *i*-th symmetrical component, is utilised. For the distributed parameter model (Fig. 3), the line parameters: $\underline{Z}_{ci}$, $\underline{\gamma}_i$ – surge impedance and propagation constant of the line SR having the length ℓ, for the *i*-th symmetrical component, is considered.

In [9] the following compact formula for the synchronisation angle has been derived:

$$A_i\cos(\delta_{Si}) + B_i\sin(\delta_{Si}) = C_i \tag{2}$$

where:

$$A_i = \text{imag}\left(\underline{Z}_{iL}^*\left((\underline{V}_{Ri} - \underline{Z}_{iL}\underline{I}_{Ri})\underline{I}_{Si}^* - \underline{V}_{Si}\underline{I}_{Ri}^*\right)\right),$$

$$B_i = \text{real}\left(-\underline{Z}_{iL}^*\left((\underline{V}_{Ri} - \underline{Z}_{iL}\underline{I}_{Ri})\underline{I}_{Si}^* + \underline{V}_{Si}\underline{I}_{Ri}^*\right)\right),$$

$$C_i = \text{imag}\left(-\underline{Z}_{iL}^*\left((\underline{V}_{Ri} - \underline{Z}_{iL}\underline{I}_{Ri})\underline{I}_{Ri}^* - \underline{V}_{Si}\underline{I}_{Si}^*\right)\right),$$

$\underline{x}^*$ – conjugate of $\underline{x}$.

There are two solutions of (2) for the synchronisation angle: δ_{Si_1}, δ_{Si_2}, if the reasonable angle range from $(-\pi)$ to $(+\pi)$ is considered [9].

After determination of the synchronization angle from (2), the distance to fault can be calculated as:

$$d_{i\_1(2)} = \text{real}\left(\frac{\underline{V}_{Si}\,e^{j\delta_{Si\_1(2)}} - (\underline{V}_{Ri} - \underline{Z}_{iL}\underline{I}_{Ri})}{\underline{Z}_{iL}(\underline{I}_{Si}\,e^{j\delta_{Si\_1(2)}} + \underline{I}_{Ri})}\right) \tag{3}$$

There are two solutions for the synchronisation angle, and two solutions are for the distance to fault (3).

Applying the distributed parameter line model, the

voltage at the fault point F, viewed from the terminals S and R, are compared, giving:

$$\underline{V}_{\mathrm{FS}i}(d_i,\delta_{\mathrm{S}i})-\underline{V}_{\mathrm{FR}i}(d_i)=0 \tag{4}$$

where:

$$\underline{V}_{\mathrm{FS}i}(d_i,\delta_{\mathrm{S}i})=\underline{V}_{\mathrm{S}i}\cosh(\underline{\gamma}_i\ell d_i)-\underline{Z}_{ci}\underline{I}_{\mathrm{S}i}\sinh(\underline{\gamma}_i\ell d_i)\mathrm{e}^{\mathrm{j}\delta_{\mathrm{S}i}}$$

$$\underline{V}_{\mathrm{FR}i}(d_i)=\underline{V}_{\mathrm{R}i}\cosh(\underline{\gamma}_i\ell(1-d_i))-\underline{Z}_{ci}\underline{I}_{\mathrm{R}i}\sinh(\underline{\gamma}_i\ell(1-d_i))$$

$\underline{\gamma}_i$, $\underline{Z}_{ci}$, ℓ – propagation constant, surge impedance of line for the *i*-th sequence, line length.

In [9] the way of solving (4) with use of the Newton-Raphson iterative calculations has been presented. As the starting point of these calculations, the results obtained according to (2)–(3) are utilised.

2.3 Subroutine SUB_A for locating faults on section AT

Fig. 4 presents the circuit diagram used for deriving the subroutine SUB_A. This subroutine is designated for locating faults FA on the line section AT.

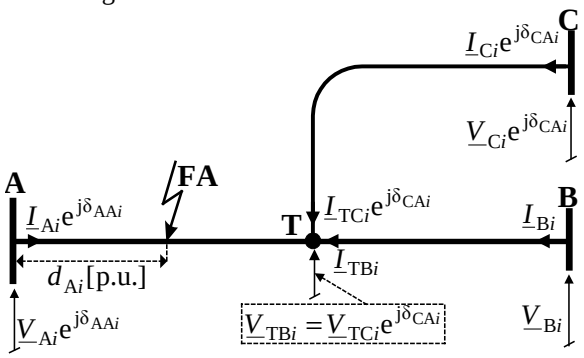

Figure 4: Subroutine SUB_A – circuit diagram for the *i*-th symmetrical component under fault at section AT.

Transferring analytically the signals from the end B towards the tap point T (Fig. 4) one obtains:

$$\underline{V}_{\mathrm{TB}i}=\underline{V}_{\mathrm{B}i}\cosh(\underline{\gamma}_{i\mathrm{LB}}\ell_{\mathrm{LB}})-\underline{Z}_{ci\mathrm{LB}}\underline{I}_{\mathrm{B}i}\sinh(\underline{\gamma}_{i\mathrm{LB}}\ell_{\mathrm{LB}}) \tag{5}$$

$$\underline{I}_{\mathrm{TB}i}=\frac{-\underline{V}_{\mathrm{B}i}}{\underline{Z}_{ci\mathrm{LB}}}\sinh(\underline{\gamma}_{i\mathrm{LB}}\ell_{\mathrm{LB}})+\underline{I}_{\mathrm{B}i}\cosh(\underline{\gamma}_{i\mathrm{LB}}\ell_{\mathrm{LB}}) \tag{6}$$

where:

$\underline{Z}_{ci\mathrm{LB}}$, $\underline{\gamma}_{i\mathrm{LB}}$ – surge impedance and propagation constant of the line section BT for the *i*-th sequence,

ℓ_{LB} – length of the line section BT.

Similarly, as in (5)–(6), the signals from the end C can be transferred analytically towards the tap point T:

$$\underline{V}_{\mathrm{TC}i}=\underline{V}_{\mathrm{C}i}\cosh(\underline{\gamma}_{i\mathrm{LC}}\ell_{\mathrm{LC}})-\underline{Z}_{ci\mathrm{LC}}\underline{I}_{\mathrm{C}i}\sinh(\underline{\gamma}_{i\mathrm{LC}}\ell_{\mathrm{LC}}) \tag{7}$$

$$\underline{I}_{\mathrm{TC}i}=\frac{-\underline{V}_{\mathrm{C}i}}{\underline{Z}_{ci\mathrm{LC}}}\sinh(\underline{\gamma}_{i\mathrm{LC}}\ell_{\mathrm{LC}})+\underline{I}_{\mathrm{C}i}\cosh(\underline{\gamma}_{i\mathrm{LC}}\ell_{\mathrm{LC}}) \tag{8}$$

where:

$\underline{Z}_{ci\mathrm{LC}}$, $\underline{\gamma}_{i\mathrm{LC}}$ – surge impedance and propagation constant of the line section CT for the *i*-th sequence,

ℓ_{LC} – length of the line section CT.

In Fig. 4 the signals (7)–(8) are synchronised analytically to the common basis (the measurements acquired at the bus B are assumed as the basis) with use of the synchronisation operator $\mathrm{e}^{\mathrm{j}\delta_{CAi}}$.

Comparing the transferred voltage (7) (after synchronising with use of the synchronisation operator ($\mathrm{e}^{\mathrm{j}\delta_{CAi}}$) and the voltage (5) one obtains the following formula for the sought synchronisation operator:

$$\mathrm{e}^{\mathrm{j}\delta_{CAi}}=\frac{\underline{V}_{\mathrm{B}i}\cosh(\underline{\gamma}_{i\mathrm{LB}}\ell_{\mathrm{LB}})-\underline{Z}_{ci\mathrm{LB}}\underline{I}_{\mathrm{B}i}\sinh(\underline{\gamma}_{i\mathrm{LB}}\ell_{\mathrm{LB}})}{\underline{V}_{\mathrm{C}i}\cosh(\underline{\gamma}_{i\mathrm{LC}}\ell_{\mathrm{LC}})-\underline{Z}_{ci\mathrm{LC}}\underline{I}_{\mathrm{C}i}\sinh(\underline{\gamma}_{i\mathrm{LC}}\ell_{\mathrm{LC}})} \tag{9}$$

Taking the signals from the end A and the signals transferred analytically to the tap point T one complets the required set of the input signals for the subroutine SUB_A. Applying the two-end algorithm from [9] (the signals specified on the left side of the below assignments) for performing the calculations of the subroutine SUB_A (the signals specified on the right side of the below assignments), we get:

$$\underline{V}_{\mathrm{S}i}\mathrm{e}^{\mathrm{j}\delta_{\mathrm{S}i}}:=\underline{V}_{\mathrm{A}i}\mathrm{e}^{\mathrm{j}\delta_{\mathrm{AA}i}} \tag{10}$$

$$\underline{I}_{\mathrm{S}i}\mathrm{e}^{\mathrm{j}\delta_{\mathrm{S}i}}:=\underline{I}_{\mathrm{A}i}\mathrm{e}^{\mathrm{j}\delta_{\mathrm{AA}i}} \tag{11}$$

$$\underline{V}_{\mathrm{R}i}:=\underline{V}_{\mathrm{TB}i} \tag{12}$$

$$\underline{I}_{\mathrm{R}i}:=\underline{I}_{\mathrm{TB}i}+\underline{I}_{\mathrm{TC}i}\mathrm{e}^{\mathrm{j}\delta_{\mathrm{CA}i}} \tag{13}$$

$\mathrm{e}^{\mathrm{j}\delta_{CAi}}$ – synchronization operator determined in (9).

Processing the signals for the subroutine SUB_A, assigned in (10)–(13), one has to take the line parameters relevant for the line section AT. This subroutine will yield two solutions for the distance to fault $d_{\mathrm{A}i\_1}$, $d_{\mathrm{A}i\_2}$ and also two solutions for the synchronization operator $\mathrm{e}^{\mathrm{j}\delta_{iA\_1}}$, $\mathrm{e}^{\mathrm{j}\delta_{iA\_2}}$. Therefore the selection will be required (provided in Section 2.6).

2.4 Subroutine SUB_B for locating faults on section TB

Fig. 5 presents the circuit diagram which is used for deriving the subroutine SUB_B, designated for locating faults FB on the line section BT.

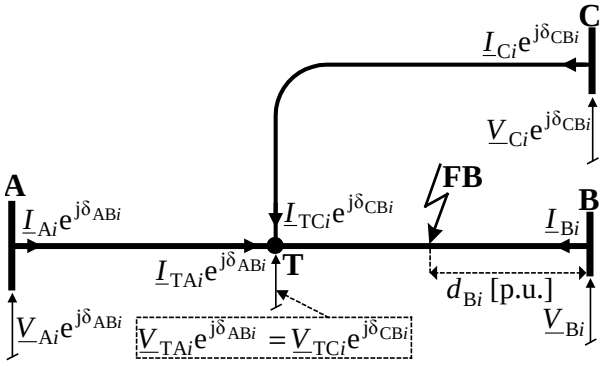

Figure 5: Subroutine SUB_B– circuit diagram for the *i*-th symmetrical component under fault at section BT.

Comparing the voltages at the tap point T (Fig. 5), one obtains the following relations between the synchronisation operators:

$$\mathrm{e}^{\mathrm{j}\delta_{CBi}}=\left(\underline{V}_{\mathrm{TA}i}/\underline{V}_{\mathrm{TC}i}\right)\mathrm{e}^{\mathrm{j}\delta_{ABi}} \tag{14}$$

$$\mathrm{e}^{\mathrm{j}(\delta_{CBi}-\delta_{ABi})}=\frac{\underline{V}_{\mathrm{A}i}\cosh(\underline{\gamma}_{i\mathrm{LA}}\ell_{\mathrm{LA}})-\underline{Z}_{ci\mathrm{LA}}\underline{I}_{\mathrm{A}i}\sinh(\underline{\gamma}_{i\mathrm{LA}}\ell_{\mathrm{LA}})}{\underline{V}_{\mathrm{C}i}\cosh(\underline{\gamma}_{i\mathrm{LC}}\ell_{\mathrm{LC}})-\underline{Z}_{ci\mathrm{LC}}\underline{I}_{\mathrm{C}i}\sinh(\underline{\gamma}_{i\mathrm{LC}}\ell_{\mathrm{LC}})}$$

where: (15)

$\underline{\gamma}_{i\mathrm{LA}}$, $\underline{Z}_{\mathrm{c}i\mathrm{LA}}$ – propagation constant and surge impedance of section AT for the *i*-th sequence,

ℓ_{LA} – section length.

Applying the two-end algorithm [9] (the signals specified on the left side of the below assignments) for performing the calculations of the subroutine SUB_B (the signals specified on the right side of the below assignments), we get:

$$\underline{V}_{\mathrm{S}i}\mathrm{e}^{\mathrm{j}\delta_{\mathrm{S}i}} := \underline{V}_{\mathrm{B}i} \tag{16}$$

$$\underline{I}_{\mathrm{S}i}\mathrm{e}^{\mathrm{j}\delta_{\mathrm{S}i}} := \underline{I}_{\mathrm{B}i} \tag{17}$$

$$\underline{V}_{\mathrm{R}i} := \underline{V}_{\mathrm{TA}i} \tag{18}$$

$$\underline{I}_{\mathrm{R}i} := \underline{I}_{\mathrm{TA}i} + \underline{I}_{\mathrm{TC}i}\mathrm{e}^{\mathrm{j}(\delta_{\mathrm{CB}i}-\delta_{\mathrm{AB}i})} \tag{19}$$

One has to take into account that on the right sides of the assignments (18)–(19) there are the signals, which are synchronised to the line end A, and not to the end B as assumed (Fig. 1). Therefore, the synchronisation angle yielded by the Subroutine SUB_B is:

$$(\delta_{\mathrm{S}i})_{\mathrm{SUB\_B}} = -\delta_{\mathrm{AB}i} \tag{20}$$

2.5 Subroutine SUB_C for locating faults on section CT

Fig. 6 presents the circuit diagram which is used for deriving the subroutine SUB_C – designated for locating faults on the line section CT.

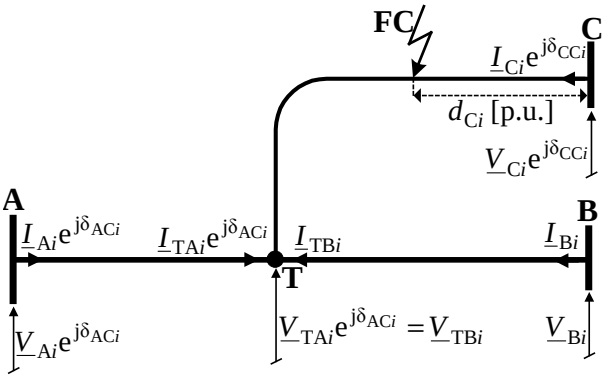

Figure 6: Subroutine SUB_C– circuit diagram for the *i*-th symmetrical component under fault at section CT.

Comparing the voltages at the tap point T (Fig. 6), which are obtained by the analytical transfer, one obtains the following relation

$$\mathrm{e}^{\mathrm{j}\delta_{\mathrm{AC}i}} = \frac{\underline{V}_{\mathrm{B}i}\cosh(\underline{\gamma}_{i\mathrm{LB}}\ell_{\mathrm{LB}}) - \underline{Z}_{\mathrm{c}i\mathrm{LB}}\underline{I}_{\mathrm{B}i}\sinh(\underline{\gamma}_{i\mathrm{LB}}\ell_{\mathrm{LB}})}{\underline{V}_{\mathrm{A}i}\cosh(\underline{\gamma}_{i\mathrm{LA}}\ell_{\mathrm{LA}}) - \underline{Z}_{\mathrm{c}i\mathrm{LA}}\underline{I}_{\mathrm{A}i}\sinh(\underline{\gamma}_{i\mathrm{LA}}\ell_{\mathrm{LA}})} \tag{21}$$

Applying the two-end algorithm [9] (the signals specified on the left side of the below assignments) for performing the calculations of the subroutine SUB_C (the signals specified on the right side of the below assignments), we get:

$$\underline{V}_{\mathrm{S}i}\mathrm{e}^{\mathrm{j}\delta_{\mathrm{S}i}} := \underline{V}_{\mathrm{C}i} \tag{22}$$

$$\underline{I}_{\mathrm{S}i}\mathrm{e}^{\mathrm{j}\delta_{\mathrm{S}i}} := \underline{I}_{\mathrm{C}i} \tag{23}$$

$$\underline{V}_{\mathrm{R}i} := \underline{V}_{\mathrm{TB}i} \tag{24}$$

$$\underline{I}_{\mathrm{R}i} := \underline{I}_{\mathrm{TB}i} + \underline{I}_{\mathrm{TA}i}\mathrm{e}^{\mathrm{j}\delta_{\mathrm{AC}i}} \tag{25}$$

2.6 Selection of valid results

The three subroutines (SUB_A, SUB_B, SUB_C) are applied in the presented fault location algorithm designed for application to a three-terminal line. Taking a particular type of symmetrical components (denoted by the subscript '*i*') each subroutine yields two solutions for the distance to fault:

- SUB_A: ($d_{\mathrm{A}i\_1}$ and $d_{\mathrm{A}i\_2}$),
- SUB_B: ($d_{\mathrm{B}i\_1}$ and $d_{\mathrm{B}i\_2}$),
- SUB_C: ($d_{\mathrm{C}i\_1}$ and $d_{\mathrm{C}i\_2}$).

Each subroutine also yields two solutions for the synchronisation angle, used for synchronising the measurements from the ends A and C:

- SUB_A: ($\delta_{\mathrm{AA}i\_1}$ and $\delta_{\mathrm{AA}i\_2}$), ($\delta_{\mathrm{CA}i\_1}$ and $\delta_{\mathrm{CA}i\_2}$),
- SUB_B: ($\delta_{\mathrm{AB}i\_1}$ and $\delta_{\mathrm{AB}i\_2}$), ($\delta_{\mathrm{CA}i\_1}$ and $\delta_{\mathrm{CB}i\_2}$),
- SUB_C: ($\delta_{\mathrm{AC}i\_1}$ and $\delta_{\mathrm{AC}i\_2}$), ($\delta_{\mathrm{CC}i\_1}$ and $\delta_{\mathrm{CC}i\_2}$).

There is a need for selecting:

- valid subroutine: SUB_A or SUB_B or SUB_C,
- valid solution of the subroutine, which has been indicated earlier as the valid one: the first solution (marked with '1' at the last position of the subscript) or the second solution (marked with '2').

The following selection indexes are applied:

$$\mathrm{SEL}_{\mathrm{LA}_i} = \frac{\mathrm{abs}(\underline{V}_{\mathrm{TB}i})}{\mathrm{abs}(\underline{V}_{\mathrm{TC}i})} \tag{26}$$

$$\mathrm{SEL}_{\mathrm{LB}_i} = \frac{\mathrm{abs}(\underline{V}_{\mathrm{TC}i})}{\mathrm{abs}(\underline{V}_{\mathrm{TA}i})} \tag{27}$$

$$\mathrm{SEL}_{\mathrm{LC}_i} = \frac{\mathrm{abs}(\underline{V}_{\mathrm{TA}i})}{\mathrm{abs}(\underline{V}_{\mathrm{TB}i})} \tag{28}$$

If there is no fault at the section AT, then the magnitudes of the phasors of voltages (for the considered *i*-th symmetrical component) at the tap point T, transferred analytically from the line ends B: $|\underline{V}_{\mathrm{TB}i}|$ and C: $|\underline{V}_{\mathrm{TB}i}|$, have to be identical (in practice very close each other). Therefore, for the fault at the section AT, we have: $\mathrm{SEL}_{\mathrm{LA}_i} \cong 1$, while the selection indexes: $\mathrm{SEL}_{\mathrm{LB}_i} \neq 1$, $\mathrm{SEL}_{\mathrm{LC}_i} \neq 1$. Analogously is for faults occurring in the other line sections. Moreover, when a given subroutine yields all results for the distance to fault (both the first and second solutions) outside its range: from 0 to 1 [p.u.], then this subroutine has to be rejected.

Selection of the valid subroutine (SUB_A or SUB_B or SUB_C) and the valid solution (the 1-st or the 2-nd) can be performed also by repeating the calculations for the other type of symmetrical components (say, the *k*-th type, where $k \neq i$), and then confronting the results of the distance to fault for these two types (*i*-th and *k*-th) of symmetrical components. The estimated distance to fault with using the *i*-th type, coinciding with the result for the *k*-th type (with some error margin) is selected as the valid result – being consistent with the actual fault.

The described selection procedure is explained in Section 3 in relation to the presented fault example.

3 ATP-EMTP ALGORITHM EVALUATION

ATP-EMTP software program [10] was applied to evaluate performance of the developed fault location algorithm. The modelled 110 kV test network includes the line sections – AT: 100 km, BT: 80 km, CT: 50 km, having the positive- and zero-sequence impedances: $\underline{Z}'_{1L} = (0.0276 + j0.315)$, $\underline{Z}'_{0L} = (0.275 + j1.027)$ (Ω/km).

The equivalent sources: $\underline{Z}_{1SA} = (0.65 + j3.69)\Omega$, $\underline{Z}_{0SA} = (1.16 + j6.57)\Omega$, $\underline{Z}_{iSB} = 2\underline{Z}_{iSA}$, $\underline{Z}_{iSC} = 3\underline{Z}_{iSA}$ were also included. Phase angles of the sources were assumed as equal to → source A: 0°, source B: –30° and source C: –15°.

In Fig. 7–Fig. 10 the fault locator input signals and the fault location results for the example fault are shown.

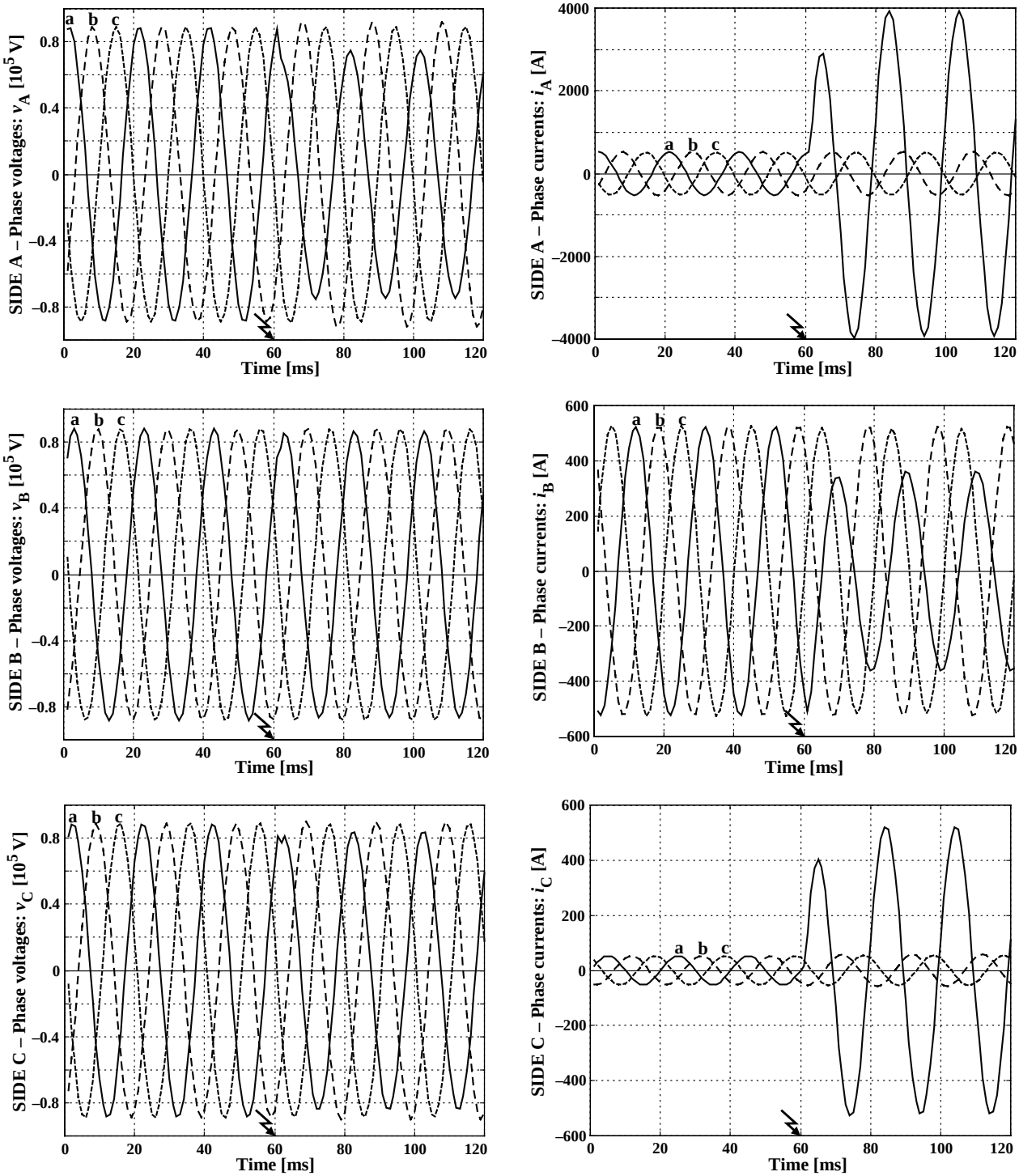

Figure 7: The fault location example – waveforms of fault locator input signals.

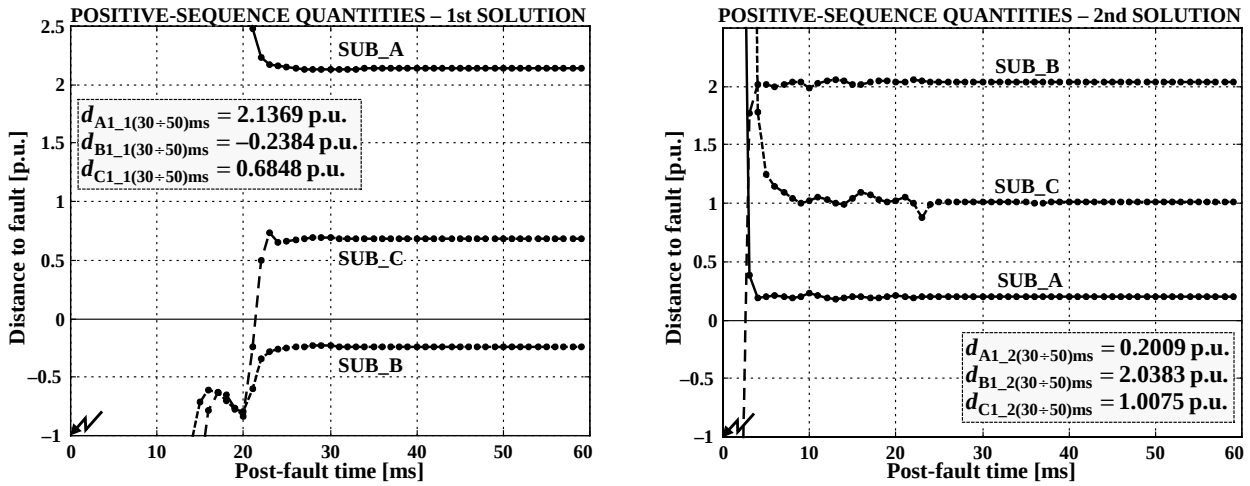

Figure 8: The fault location example – the 1st and 2nd solutions for the distances to fault applying positive-sequence quantities.

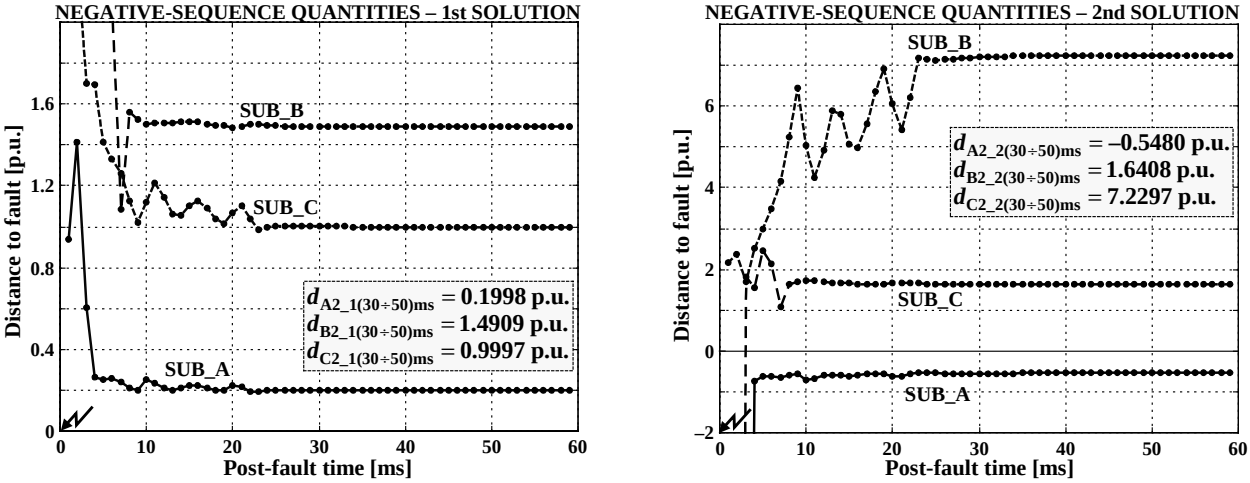

Figure 9: The fault location example – the 1st and 2nd solutions for the distances to fault applying negative-sequence quantities.

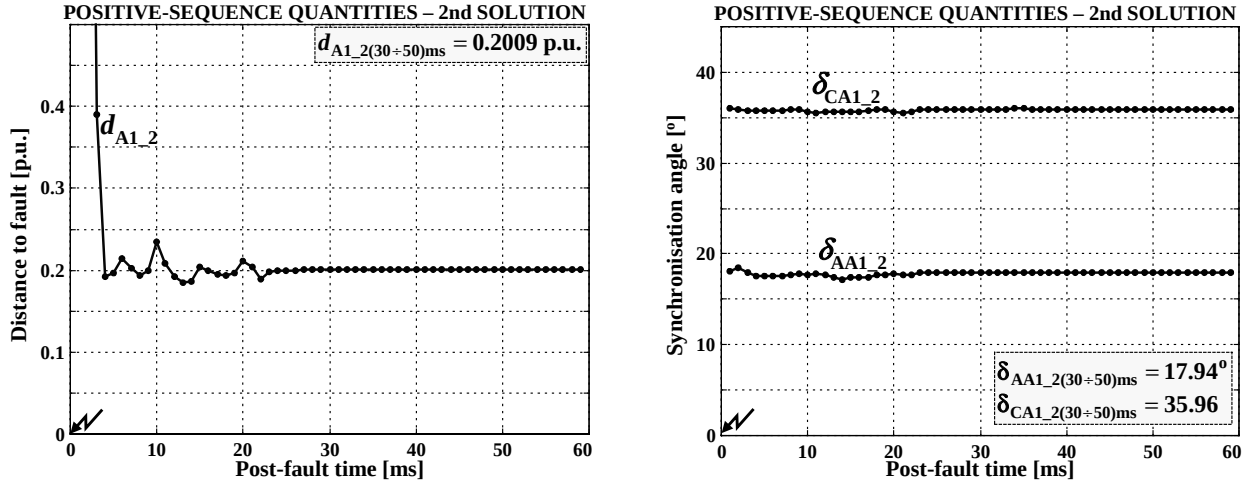

Figure 10: The fault location example – the results (the 2nd solutions for use of the positive-sequence quantities) for the distance to fault and for the synchronisation angles of measurements from the ends A and C, selected as the valid results.

The specifications of the fault from the example presented in Fig.7–Fig. 10 are as follows:

- fault type: a-g,
- fault resistance: 10 Ω,
- faulted section: AT,
- fault distance: d_A=0.2 p.u.

The current and voltage signals from the line end A were intentionally delayed by a single sample, while the signals from the end C by two samples. Such delays for the applied sampling frequency of 1000 Hz correspond

to the case of unsynchronised measurements with the synchronisation angles equal to: $\delta_A=18^o$, $\delta_C=36^o$.

For evaluating the accuracy of the presented fault location algorithm itself, the errorless current and voltage transformers were modelled. Analogue anti-aliasing filters with the cut-off frequency of 350 Hz were included (1 kHz sampling frequency was used). Full-cycle Fourier orthogonal filters were applied. The obtained continuous time results were averaged within the post-fault interval: from 30 up to 50 ms.

Input signals for the presented example are shown in Fig. 7. In Fig. 8 there are the results of a distance to fault calculation using the positive-sequence quantities: the 1st solution indicates the fault on the section CT (SUB_C: d_{C1_1}=0.6848 p.u.), while the 2nd solution the fault on the section AT (SUB_A: d_{A1_2}=0.2009 p.u.). Using the selection indexes (26)–(28), the subroutine SUB_A undergoes indicated as the valid one, for which the 2nd solution yields the result d_{A1_2} being very close to the actual distance to fault: d_A=0.2 p.u. Also, the selection can be performed by repeating the calculations for the other type of sequence component, as for example for the negative-sequence (Fig. 9). Confronting the results from Fig. 8 with those shown in Fig. 9, one gets that the result: d_{A1_2}=0.2009 p.u. is confirmed by the result: d_{A2_1}=0.1998 p.u. (as being the most closer) as the valid one. In Fig. 10 the valid results are shown. The errors are very low: 0.0009 p.u. (for the fault distance) and 0.06° (for the angle $\delta_A=18^o$) and 0.04 (for the angle $\delta_C=36^o$).

Besides the presented example, an extensive evaluation study has been performed. Different specifications of faults have been considered in the study. For example, in the synthetic evaluation for the population of 108 fault cases:

- 4 fault types (a-g, a-b, a-b-g, a-b-c),
- faults on each of 3 sections (AT, BT, CT),
- faults at 9 locations (from 0.1 to 0.9 p.u.)

the following maximal errors in fault distance calculation were achieved:

- for the lumped line model (starting point for iterative calculations with the distributed parameter line model): 1.01%
- for the distributed parameter line model: 0.14%.

Note: a fault resistance of 10 Ω for single phase faults and 1 Ω for inter-phase faults was applied.

The achieved accuracy is very high, especially for the use of the distributed parameter line model. Reliable selection of the valid results was obtained as well.

Implementing this method to the real fault location device, also the errors caused by non-ideal transformation of instrument transformers have to be accounted for.

4 CONLUSIONS

New fault location algorithm for three-terminal line utilising unsynchronised measurements of three-end currents and voltages has been derived. The algorithm consists of three subroutines and the procedure for selecting the valid result. The distributed parameter line model is strictly taken into account for deriving the algorithm subroutines. The calculations are performed for a particular type of symmetrical component, as for example for the positive-sequence.

There is a need for selecting the valid result, which is consistent with the actual fault. The selection indexes can be used for that. Also, the selection can be performed by additional use of the other type of components, as in the presented example.

The presented results of the ATP-EMTP evaluation prove the validity of the derived algorithm. The obtained accuracy of fault location is comparable with the achieved when using synchronised measurements.

REFERENCES

[1] R.K. Aggarwal, D.V. Coury, A.T. Johns and A. Kalam, “A practical approach to accurate fault location on extra high voltage teed feeders”, IEEE Trans. Power Delivery, Vol. 8, pp. 874–883, July 1993

[2] A.A. Girgis, D.G. Hart and W.L. Peterson “A new fault location technique for two-and three-terminal lines”, IEEE Trans. Power Delivery, Vol. 7, No.1, pp. 98–107, January 1992

[3] D. A. Tziouvaras, J. Roberts and G. Benmmouyal, “New multi-ended fault location design for two- or three-terminal lines”, Proceedings of 7th International IEE Conference on Developments in Power System Protection, pp. 395–398, April 2001

[4] Y. Lin, C. Liu and C. Yu, “A new fault locator for three-terminal transmission lines using two-terminal synchronized voltage and current phasors”, IEEE Trans. Power Delivery, Vol. 7, No.3, pp. 452–459, July 2002

[5] J.F. Minambres, I. Zamora, A.J. Mazon, M.A. Zorrozua and R. Alvarez-Isasi, “A new technique, based on voltages, for fault location on three-terminal transmission lines”, Electric Power Systems Research 37, pp 143–151, 1996

[6] S.M. Brahma, “Fault Location Scheme for a Multi-Terminal Transmission Line Using Synchronized Voltage Measurements”, IEEE Trans. on Power Delivery, Vol. 20, No. 2, pp. 1325–1331, April 2005

[7] J. Izykowski, R. Molag, E. Rosolowski and M.M. Saha, “Fault location in three-terminal line with use of limited measurements”, CD Proceedings of PowerTech, St. Petersburg, June 2005

[8] J. Izykowski, E. Rosolowski, M.M. Saha, M. Fulczyk and P. Balcerek, “A fault location method for application with current differential relays of three-terminal lines”, IEEE Trans. on Power Delivery, Vol. 22, No. 4, pp. 2099–2107, October 2007

[9] J. Izykowski, R. Molag, E. Rosolowski and M.M. Saha, “Accurate location of faults on power transmission lines with use of two-end unsynchronized measurements” IEEE Trans. on Power Delivery, Vol. 21, No. 2, pp. 627–633, April 2006

[10] H.W. Dommel, Electro-Magnetic Transients Program, BPA, Portland, Oregon, 1986.